Metallurgical characterisation of B2 Ti-based binary alloys with Group VIIIB transition metals

Bongani Ngobe[1*, 2], *Mahlaga* Molepo[2], *Ramogohlo* Diale[1], *Donald* Mkhonto[1], and *Maje* Phasha[1]

[1]Advanced Materials Division, MINTEK, Private Bag X 3015, Randburg, 2125, South Africa
[2]School of Physics, University of the Witwatersrand, Private Bag 3, Wits, 2050, South Africa

Abstract. B2-CsCl intermetallic compounds exhibit excellent high-temperature stability, corrosion resistance, and mechanical strength. During solidification, these compounds can recrystallise and undergo martensitic phase transformation, a phenomenon widely studied in TiNi and associated with shape memory behaviour. In contrast, the B2 phase of TiRu, with Ru being the least expensive platinum group metal, remains thermodynamically stable down to room temperature, showing no phase change, and is thus not a high-temperature shape memory alloy. This raises a key research question: why does B2 TiRu not exhibit transformation behaviour comparable to TiNi and TiPd, and how does its experimental phase stability differ? This study investigated the metallurgical characterisation of TiRu, TiNi, and TiPd alloys produced via arc melting under argon. X-ray diffraction (XRD) confirmed the stable B2 phase in TiRu, while TiNi and TiPd exhibited multiple secondary phases, indicating B2 instability and potential phase transformations at lower temperatures. Micro-Vickers hardness measurements and optical microscopy revealed relationships between microstructure and mechanical response. Hardness of TiNi and TiPd improved upon annealing due to grain refinement, whereas TiRu softened, likely due to grain coarsening.

1 Introduction

Titanium (Ti) based intermetallic alloys consisting of B2 (CsCl-type) phase with space group Pm-3m (#221), have gained significant attention due to their superior high-temperature stability, corrosion resistance, and mechanical properties, making them ideal candidates for aerospace and high-temperature structural applications [1-3]. B2 alloys are broadly classified based on their phase stability, with some undergoing martensitic phase transformation (MPT), a characteristic widely observed in TiNi alloy, while others, such as TiRu, retain their B2 crystal structure at room temperature [4]. This martensitic phase transformation, particularly in the Ti-Ni system at composition near equiatomic, is well known to proceed through a two-step process, starting from B2 austenite to monoclinic B19′, with an intermediate B19 orthorhombic phase [5].

* Corresponding author: Bonganing@mintek.co.za & 2623288@students.wits.ac.za

Figures 1 and 2 present the binary phase diagrams of the TiNi, TiPd, and TiRu systems. Common to all is the formation of a B2 phase at high temperatures, and upon cooling, the behaviour of this B2 phase differs significantly among these compounds. In the TiNi and TiPd systems, as illustrated in Figures 1(a) and 1(b), their B2 phase becomes unstable at lower temperatures, resulting in the formation of low-symmetry phases such as B19, B19', or other intermetallic compounds. This is a clear indication that the B2 of these compounds is likely to undergo martensitic phase transformation at lower temperatures. In contrast, the binary phase diagram of TiRu given in Figure 2 reveals only the presence of the B2 phase. This indicates that the B2 of TiRu remains thermodynamically stable, retaining its sole B2 phase throughout the solidification range without undergoing any phase transformation. This behaviour differs from the TiNi and TiPd binary systems [6-8].

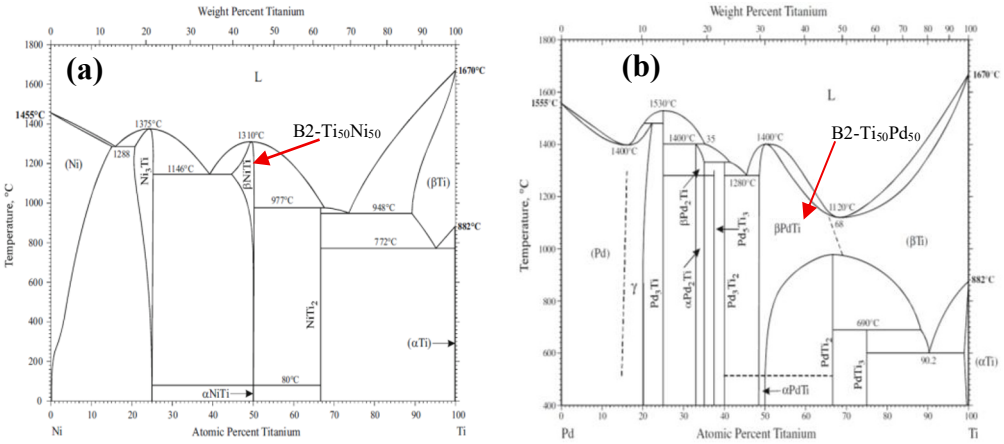

Fig. 1. TiNi and TiPd binary phase diagrams [6, 8]. Figure 1(a) reprinted from J. L. Murray, Ni–Ti (nickel–titanium). Binary Alloy Phase Diagrams, 2nd ED., ed. T. B. Massalski, **3**, 1763–1767 (1986). And Figure 1(b) is reprinted from H. Okamoto, Pd-Ti (Palladium-Titanium). J. Phase Equilib. Diffus. **34**, 74–75 (2013).

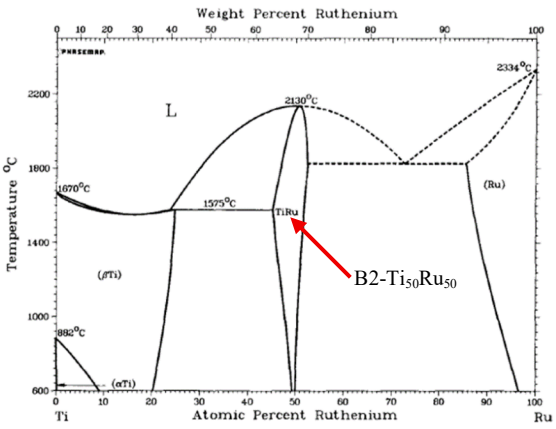

Fig. 2. The binary phase diagram of TiRu alloy [7]. J.L. Murray, The Ru-Ti (ruthenium-titanium) System. Bulletin of Alloy Phase Diagrams. **3**, 216-221 (1982)

Nitinol (TiNi) is a widely studied shape memory alloy (SMA) due to its remarkable shape memory effect (SME) and pseudo-elasticity (PE), rendering it ideal for applications in biomedical, actuator, and aerospace industries. However, Nitinol has limitations, including low transformation temperatures (~100 °C), poor high-temperature mechanical properties, and oxidation resistance, restricting its use in extreme environments [3,9].

To address these challenges, our previous studies employed density functional theory (DFT) calculations to investigate the MPT behaviour of these three binary alloys, including B2 TiPt [9-10]. In addition, the incorporation of Group 10 transition metals (Ni, Pd and Pt) into the stable B2 TiRu system to induce MPT and improve its martensitic transformation characteristics was explored [12-14]. Theoretical predictions suggest that alloying B2 TiRu with the above-mentioned transition metals impacts its stability and enables phase transition [12-14]. However, experimental validation is required to assess the accuracy of these predictions and their practical implications.

Drawing from the previous theoretical observations, the current study presents the initial experimental effort to manufacture and characterise three Ti-based B2 binary alloys, namely, TiNi, TiRu, and TiPd. The objective is to investigate their equilibrium phase stability and phase transformation behaviour using metallurgical characterisation techniques. The findings of this study aim to increase the understanding of equiatomic B2 intermetallic alloys, particularly in the context of high-temperature and shape memory applications.

2 Experimental procedures

2.1 Alloys production and annealing

Button ingots of 20g each of the three investigated B2 Ti-based binary alloys were produced using a state-of-the-art AMAZEMET arc melting technique, shown in Figure 3. High-purity titanium and Group VIIIB metallic powders were arc-melted in the AMAZEMET system equipped with a tungsten electrode and a water-cooled copper hearth. The melting process was conducted under a controlled argon atmosphere to prevent oxidation. To ensure chemical homogeneity, each ingot was flipped and re-melted at least three times.

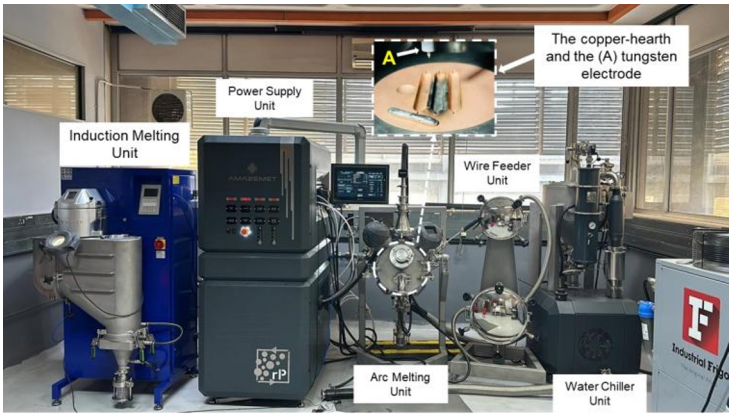

Fig. 3. The AMAZEMET® system used for melting button ingots in this study, with all the essential units labelled [15].

After melting, representative samples with dimensions of 10 × 10 × 5 mm were sectioned from the respective button ingots using electric discharge machining (EDM). For each alloy (TiNi, TiPd, and TiRu), two sectioned samples were prepared, one retained in the as-cast

condition and the other subjected to annealing. The annealed labelled samples were placed into the Carbolite-Gero® vertical tube furnace set to 1100 °C, with a heating rate of 10 °C/min under a controlled Argon atmosphere. The samples were solution treated at this temperature for 1 hour and then allowed to cool to room temperature within the furnace.

2.2 Metallography preparation and phase identification

All six samples, representing both the as-cast (AC) and annealed (AN) conditions, were mounted in black resin, uniquely labelled, and ground using SiC abrasive papers. Thereafter, polished down to a 1µm mirror-like surface finish suitable for metallurgical characterisation.

The prepared samples' surfaces were etched using a modified Kroll's reagent solution (10% HF, 10% HNO_3 and 80% H_2O). Kroll's reagent is widely recognised for its effectiveness in revealing the microstructural features of titanium and its alloys. However, the presence of platinum group metals (PGMs) in TiPd and TiRu renders this reagent ineffective to expose their underlying microstructures. Thus, the aqua-regia solution of 75% HCl and 25% HNO_3 was considered for these two binary alloys, and still, TiRu could not be attacked by either Kroll's or the aqua-regia reagents.

Additionally, phase identification and crystal properties of the investigated alloys were conducted using X-ray diffraction. XRD is a non-destructive analytical technique capable of identifying crystalline phases and determining structural properties such as lattice parameters [16].

XRD scans were performed on the as-polished surfaces of the investigated B2 binary compounds using a Bruker D8® X-Ray diffractometer equipped with a CoKα X-ray source (λ=1.78897 Å). Data capturing was set with a step increment of 0.02° per second in a non-rotating mode, ranging from 5° to 80° of the 2θ angle.

Thereafter, the collected XRD patterns were analysed using EVA® software (Bruker's evaluation software for XRD data analysis) for peak identification. Subsequently, the phase identification and peaks matching were performed using the International Centre of Diffraction Data (ICDD) PDF-2 2003 database.

2.3 Hardness measurement

Additionally, the as-cast and the annealed samples were subjected to hardness measurement using a Falcon® 400 micro-Vickers hardness tester. Five random indentations were made on the prepared surfaces of the mounted samples using a load of 2 kg (HV_2) with a dwelling time of 15s. Hardness data have a close relationship with a material's mechanical properties, such as strength and ductility. Hence, for solid materials, it is regarded as a measurement of their resistance to permanent shape change when a constant compressive load is applied [17].

3 Results and discussions

3.1 Microstructural results

Figures 4 to 6 display the optical microscope (OM) micrographs of the investigated TiNi, TiPd, and TiRu binary compounds.

Figure 4 (a) and (b) show the OM microstructures of the AC and AN TiNi samples, respectively. In the AC condition shown in Figure 4(a), there are distinct dendritic grains. This formation results from the rapid cooling during solidification in the casting process, which leads to a noticeable retention of the high-temperature B2 phase down to room temperature. Such retention reflects a metastable condition, temporarily preserved by the fast

cooling, rather than true equilibrium stability. The microstructure also reveals phases of darker and lighter contrast at the slightly coarser grain boundaries. This indicates segregation into nickel-rich and titanium-rich phases within the grains, which can be attributed to narrow compositional variations and uneven cooling rates during the solidification (see Figure 1(a)) [18].

The annealing process was undertaken to ensure elemental segregation is eliminated and to refine the phase distribution resulting from the rapid solidification of non-equilibrium microstructures, such as retained and metastable phases. This process promotes the recovery and recrystallisation of microstructural phases, leading to refined and uniformly dispersed grains within the matrix and facilitating the precipitation of secondary phases [19]. Hence, it is a well-known fact that the strength and hardness of conventional metals increase as grain size decreases, a fundamental concept described as the Hall-Petch effect [20].

In Figure 4(b), the annealing process appears to have reduced the grain size, resulting in grains that are more evenly distributed across the matrix [19]. This may have a strengthening effect on the properties of the annealed sample, as secondary phases are homogeneously diffused.

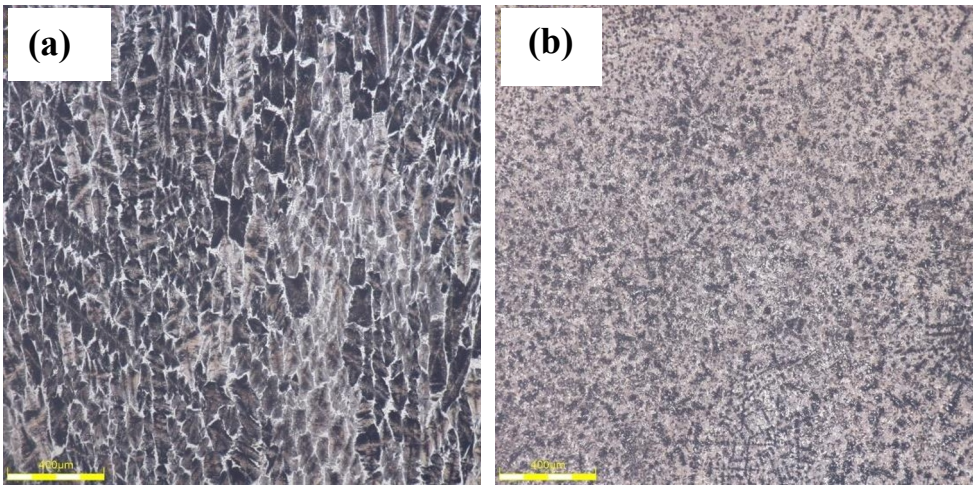

Fig. 4. The optical microscope micrographs of TiNi, representing the (a) as-cast and (b) annealed conditions, respectively.

Figure 5(a) and (b) illustrate the microstructures of the AC and AN TiPd samples, respectively. As shown in the binary phase diagram in Figure 1(b), the B2 phase of TiPd solidifies over a broader compositional range than TiNi. This broader window can promote the formation of secondary phases during solidification at uneven rates.

In Figure 5(a), the phases are distributed heterogeneously, though the grains appear fine. In contrast, Figure 5(b) demonstrates that the annealing process significantly refines the grains, leading to a more homogeneous distribution of the phases. However, this refinement may only have a limited effect on the material's overall strengthening, since the grain sizes remain relatively similar between the AC and AN conditions, and other factors such as precipitation also play a role.

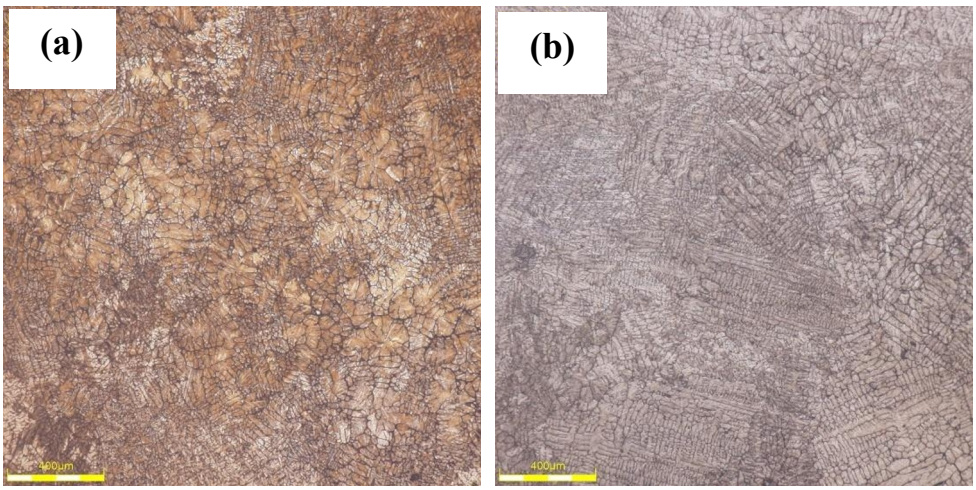

Fig. 5. The optical microscope micrographs of TiPd, representing the (a) as-cast and (b) annealed conditions, respectively.

As mentioned in Section 2.2, neither Kroll's reagent nor the aqua regia solution successfully revealed the microstructure of the TiRu binary representative under the annealed condition. Only the as-cast sample showed observable features, which appear relatively homogenised with finely dispersed grains throughout the matrix. Consequently, this limited observation illustrated in Figure 6 presents only the AC microstructure, consistent with the known stability of the B2 phase of TiRu down to room temperature, with no detectable secondary phases [10-14]. In contrast, the B2 phases of TiNi and TiPd are naturally less stable and tend to develop secondary phases, leading to phase transformations at lower temperatures, see Figure 1(a) and (b).

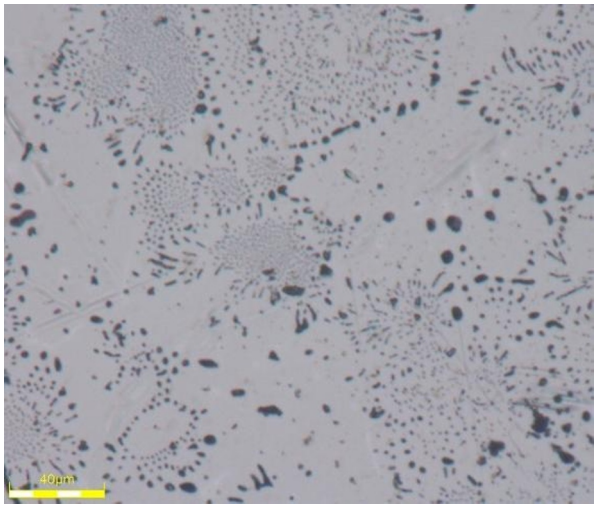

Fig. 6. The optical microscope micrograph of TiRu representing the as-cast condition.

3.2 XRD phase identification results

Figures 6 and 7 present the XRD patterns for the TiNi, TiPd, and TiRu compounds investigated. Figure 6(a) illustrates the TiNi system, while Figure 6(b) shows the TiPd

system, both presented in their AC and AN conditions, respectively. Meanwhile, Figure 7 presents the XRD patterns of the TiRu system in its as-cast condition.

In the bottom panel of Figure 6(a), three phases were detected in the TiNi-AC sample, confirming the presence of a high-temperature B2-TiNi phase (cubic, Pm-3m, #221), the low-temperature $NiTi_2$ (cubic, Fd-3m, #227), which is associated with a martensitic phase, as well as the presence of the α-Ti phase. The AC results reported here agreed with the work reported by Jones et al. [21]. On the other hand, the top panel of Figure 6(a) shows the presence of five intermetallic phases in the TiNi-AN sample. This confirms the presence of B19′ TiNi (monoclinic, $P2_1/m$, #11), B2-NiTi (cubic, Pm-3m, #221), $NiTi_2$ (cubic, Fd-3m, #227), Ni_3Ti (hexagonal, P63/mmc, #194) and Ni_4Ti_3 (hexagonal, R-3, #148) phases.

The XRD pattern on the bottom panel of Figure 6(b) reveals four distinct intermetallic phases in the TiPd-AC sample. These include the presence of B2-PdTi (cubic, Pm3m, #221), Pd_2Ti (tetragonal, I4/mmm, #139), PdTi (orthorhombic, Pmma, #51), and Pd_3Ti (hexagonal, P63/mmc, #194) phases. Additionally, the top panel of Figure 6(b) shows five distinct phases identified in the TiPd-AN sample, confirming the presence of PdTi (orthorhombic, Pmma, #51), $TiPd_3$ (hexagonal, P63/mmc, #194), Pd_2Ti (tetragonal, I4/mmm, #139), as well as α (HCP) and γ (FCC) solid solutions.

In Figure 7, a sole intermetallic phase was identified as the B2-TiRu (cubic, Pm-3m, #221). The stability of B2 TiRu persists down to room temperature, with no detectable secondary phases.

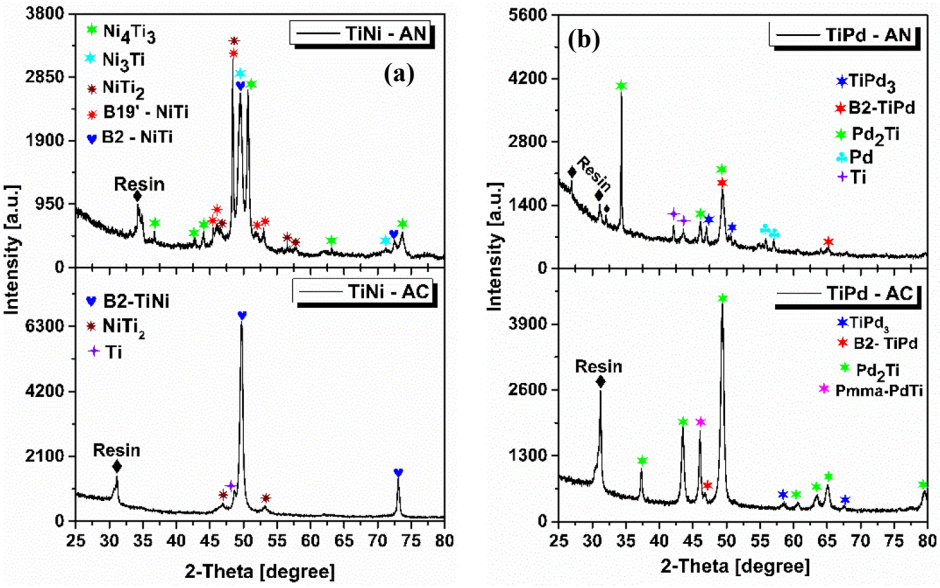

Fig. 6. The XRD patterns of the B2 TiNi and TiPd compounds, in their as-cast and annealed conditions, respectively.

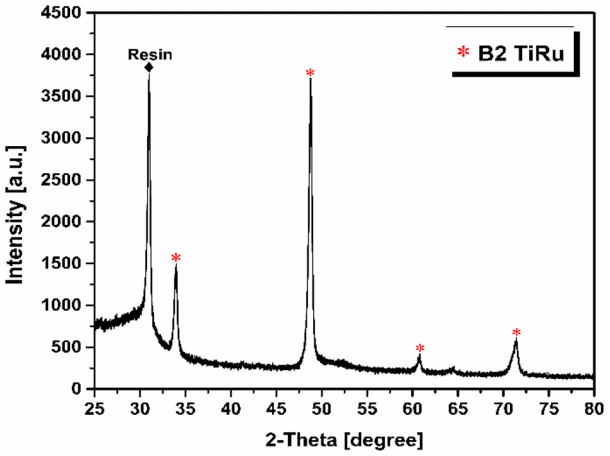

Fig. 7. The XRD patterns of the B2 TiRu compound in the as-cast condition.

The reported XRD results agree well with the microstructural features observed in Section 3.1, as well as the phases present in the respective binary phase diagrams (see Figures 1 and 2). Furthermore, all the XRD patterns reported here consist of a common peak at around 30° in the 2θ position, identified as graphite from the mounting resin.

3.3 Vickers hardness results

Figure 8 presents the micro-Vickers hardness results obtained from the investigated B2 compounds. The graph displays the average HV_2 values plotted along with error bars reflecting the standard deviation for both the as-cast and annealed representative samples. It is well known that the strength or hardness of conventional metals increases with decreasing grain size, a fundamental concept well outlined by the Hall-Petch principle [20].

For B2 TiNi, the Vickers hardness values were found to increase from an average of 235.5 to 390.1 HV_2 for the AC and AN samples, respectively. This significant hardening effect observed after annealing is likely due to enhanced ordering of the B2 phase, and the precipitation of Ni_3Ti, B19' and Ni_4Ti_3 intermetallic phases as shown in Figure 6 (a). The small error bars indicate the consistency of the reported results, which can be attributed to possible phase uniformity and minimal segregation.

In the case of B2 TiPd, the hardness values were found to average at 259.6 and 308.8 HV_2 for both the AC and AN samples, respectively. As shown in Figure 8, the moderate hardening effect observed after annealing suggests that the B2 phase remained relatively stable throughout the process. This is also the evidence with the low error bars observed. The slight increase in hardness may be attributed to the segregation of the martensitic Pmma-PdTi phase into elemental Pd and Ti phases, as shown by the XRD peaks given in Figure 6(b). This may result from the reduced internal strain due to annealing, a common characteristic observed in TiPd-based shape memory alloys [1-2].

For B2 TiRu, an opposite trend was observed, with average values of 475.1 and 392.9 HV_2 for AC and AN samples, respectively. As shown in Figure 6, the AC microstructure reveals grain boundary precipitates, which may be evidence of the high hardness of B2 in its AC condition. This suggests that the B2 phase in TiRu remains relatively stable even at room temperature, as theoretically expected [22]. The annealing process introduced some softening to the compound, likely due to the grain coarsening of the dominant B2 phase throughout the matrix, which is reflected by the hardness reduction on the AN sample.

Although Figure 7 shows that only B2 was detected in the XRD pattern, other phases, such as Ti-rich or Ru-rich, might be present, judging from the agglomerated dark contrasts on the grain boundaries of the microstructure shown in Figure 6. These possible phases, if present, may be either thermodynamically unstable or they are below the XRD detection limit (~2 wt.%). Efforts to ascertain this will form part of our future work to study these metastable phases using a scanning electron microscope (SEM) [23]. These observations agree with a DFT study conducted by Xing et al., which reported the possible existence of other metastable phases in TiRu, such as Ru_2Ti, $RuTi_3$, and $TiRu_3$ [24-25]. However, to date, there is no experimental work that has been conducted to verify the existence of such metastable phases.

Though the hardness results reported here were found to differ from those reported by other researchers, such as 216 HV_{50} for B2 TiNi, 262 HV_{50} for B2 TiPd and 699 HV_{50} for B2 TiRu, the general trends observed were found to be in good agreement [26]. Furthermore, the hardness results reported here are in support of the microstructural morphology shown in Figures 4 to 6, as discussed in Section 3.1.

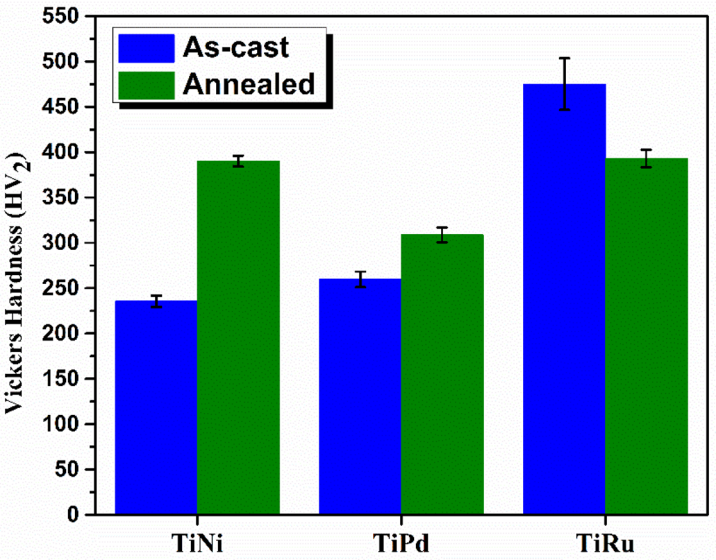

Fig. 8. The Vickers hardness results of the investigated B2 compounds.

4 Conclusions

This study successfully carried out the metallurgical characterisation of TiNi, TiPd, and TiRu alloys in both as-cast conditions. The XRD analysis confirmed and identified the presence of some retained B2, orthorhombic, and hexagonal phases, which were found to correlate well with the microstructural features observed in the optical microscope. This was eventually validated by the micro-Vickers hardness profile obtained. These results provide vital information about the shape memory effect in TiNi and TiPd. While B2 TiRu remains stable at room temperature, exhibiting no phase transformation, B2 of TiNi and TiPd upon cooling decompose into secondary phases, indicating a possible phase transformation. Future work will involve the assessment of mechanical properties and transformation behaviour of these B2 compounds using Differential Scanning Calorimetry (DSC) and verifying the existence of the metastable phases in the TiRu binary system using SEM coupled with Energy Dispersive Spectroscopy (EDS) analysis.

This work is published with the permission of MINTEK and the University of the Witwatersrand. The authors are grateful for the financial support provided by the Advanced Metals Initiative (AMI) of the Department of Science and Innovation (DSI), South Africa. Computational resources were generously provided by the Centre for High-Performance Computing (CHPC), Cape Town, which enabled the remote execution of simulations and data analysis.

Data availability: Data supporting the findings of this study can be made available by the corresponding authors upon reasonable request, subject to MINTEK's confidentiality policy.

References

1. K. Otsuka, X. Ren, Recent developments in the research of shape memory alloys. Intermetallics. **7**, 511–528 (1999). https://linkinghub.elsevier.com/retrieve/pii/S0966979598000703
2. K. Otsuka, X. Ren, Physical metallurgy of Ti-Ni-based shape memory alloys. Prog. Mater. Sci. **50**, 511-678 (2005). https://doi.org/10.1016/j.pmatsci.2004.10.001
3. J. Ma, I. Karaman, R. D. Noebe, High temperature shape memory alloys. Int. Mater. Rev. **55**, 257–315 (2010). https://doi.org/10.1179/095066010X12646898728363
4. C. Frey et al., High temperature B2 precipitation in Ru-containing refractory multi-principal element alloys. Metall. Mater. Trans. A **55**, 1739–1764 (2024). https://doi.org/10.1007/s11661-024-07368-x
5. A. Wadood, Titanium and titanium alloys. Higher Education Commission, Pakistan, 2018.
6. H. Okamoto, Pd-Ti (Palladium-Titanium). J. Phase Equilib. Diffus. **34**, 74–75 (2013). https://doi.org/10.1007/s11669-012-0137-6
7. J.L. Murray, The Ru-Ti (Ruthenium-Titanium) System. Bull. Alloy Phase Diagrams. **3**, 216-22 (1882). https://doi.org/10.1007/BF02892392
8. J. L. Murray, Ni–Ti (nickel–titanium). Binary Alloy Phase Diagrams, 2nd ED., ed. T. B. Massalski, **3**, 1763–1767 (1986). American Society for Metals. ISBN: 978-0-87170-261-6.
9. Y. Yamabe-Mitarai, TiPd- and TiPt-based high-temperature shape memory alloys: a review on recent advances. Metals **10**, 1–21 (2020). https://doi.org/10.3390/met10111531
10. B. S. Ngobe, M. J. Phasha, R. G. Diale, M. P. Molepo, The phase stability, mechanical and electronic properties of CsCl-type intermetallic: $Ti_{50}TM_{50}$ (TM = Ni, Ru and Pd), a first-principles approach. The 66th SAIP Conf. Proc., 81–87 (2022). https://events.saip.org.za/event/225/page/546-the-proceedings-of-saip2022
11. B. Ngobe et al., Ab-initio techniques, VASP and CASTEP, are used to investigate the electronic properties of B2 compounds formed between Ti and group VIII elements - a comparative study. MATEC Web Conf. **370**, 1–10 (2022). https://doi.org/10.1051/matecconf/202237002005
12. B. Ngobe, M. Molepo, M. Phasha, First-principles study on the effect of Ni addition on the stability of B2 $Ti_{50}Ru_{50}$ – a supercell approach, MATEC Web Conf. **388**, 1–10 (2023). https://doi.org/10.1051/matecconf/202338807017

13. B. Ngobe, M. Molepo, D. Mkhonto, M. Phasha, Effect of Pd substitution on elastic and lattice dynamic properties of B2 $Ti_{50}Ru_{50}$ - ab initio study. MATEC Web Conf. **406**, 1–9 (2024). https://doi.org/10.1051/matecconf/202440606002
14. B. S. Ngobe, M. J. Phasha, M. P. Molepo, I. A. Mwamba, First-principles study of $Ti_{50}Ru_{50-x}Y_x$ (Y = Ni, Pd and Pt) with a prospect to induce SME on stable CsCl-type $Ti_{50}Ru_{50}$ phase. MRS Adv. **8**, 645–650 (2023). https://doi.org/10.1557/s43580-023-00573-7
15. Ł. Żrodowski et al., Novel Cold Crucible Ultrasonic Atomization Powder Production Method for 3D Printing. Materials. **14**, 1-11 (2021). https://doi.org/10.3390/ma14102541
16. G. Will, Powder diffraction: the rietveld method and the two-stage method to determine and refine crystal structures from powder diffraction data. Springer (2006). ISBN: 978-3-540-27986-0
17. E. Broitman, Indentation hardness measurements at macro-, micro-, and nanoscale: a critical overview. Tribol. Lett. **65**, 23 (2017). https://doi.org/10.1007/s11249-016-0805-5
18. N. El-Bagoury, M.M. Hessien, Z.I. Zaki, Influence of aging on microstructure, martensitic transformation and mechanical properties of NiTiRe shape memory alloy. Met. Mater. Int. 20, 997-1002 (2014). https://doi.org/10.1007/s12540-014-5003-0
19. S. Guha, I. Baker, P.R. Munroe, J.R. Michael, The effect of annealing on Ni-Al-Fe B2 compounds. Mater. Sci. Eng. A **152**, 258–263 (1992). https://doi.org/10.1016/0921-5093(92)90076-D
20. J. Hu et al., Grain boundary stability governs hardening and softening in extremely fine nanograined metals. Science, **355**, 1292-1296 (2017). https://doi.org/10.1126/science.aal5166
21. N. G. Jones, S. L. Raghunathan, D. N. Dye, In-situ synchrotron characterization of transformation sequences in TiNi-based shape memory alloys during thermal cycling. Metall. Mater. Trans. A. **41**, 912–921 (2010). https://doi.org/10.1007/s11661-009-0166-x
22. H. C. Donkersloot, J. H. N. Van Vucht, Martensitic transformations in gold-titanium, palladium-titanium and platinum-titanium alloys near the equiatomic composition. J. Less-Common Met. **20**, 83–91 (1970). https://doi.org/10.1016/0022-5088(70)90092-5
23. J. A. Newman et al., Parts per million powder x-ray diffraction. Anal. Chem. **87**, 10950–10955 (2015). https://doi.org/10.1021/acs.analchem.5b02758
24. M. Jahnatek et al., Ordered phases in ruthenium binary alloys from high-throughput first-principles calculations. Phys. Rev. B. **84**, 214110 (2011). https://doi.org/10.1103/PhysRevB.84.214110
25. W. Xing et al., First-principles studies of structural stabilities and enthalpies of formation of refractory intermetallics: TM and TM_3 (T = Ti, Zr, Hf; M = Ru, Rh, Pd, Os, Ir, Pt). Intermetallics. **28**, 16-24 (2012). https://doi.org/10.1016/j.intermet.2012.03.033
26. R. M. Waterstrat, R. Kuentzler, Structural instability in the B2-type ordered alloys Zr (Ru, Rh) and Zr (Ru, Pd). J. Alloys Compd. **359**, 133–138 (2003). https://doi.org/10.1016/S0925-8388(03)00187-7